International Journal of Fracture (2005) 135:187–197
DOI 10.1007/s10704-005-3949-0

Biological structures mitigate catastrophic fracture through various strategies

R. BALLARINI[1,*], R. KAYACAN[2], F.-J. ULM[3], T. BELYTSCHKO[4] and A.H. HEUER[1]
[1]*Case Western Reserve University, Civil Engineering, 10900 Euclid Avenue, Cleveland, OH 44106-7201, USA*
[2]*Suleyman Demirel University*
[3]*Massachusetts Institute of Technology*
[4]*Northwestern University*
[*]*Author for correspondence. (E-mail: roberto.ballarini@case.edu)*

Received 4 July 2005; accepted in revised form 10 October 2005

Abstract. Gao et al. (PNAS, **100**, 5597–5600 (2003)) have argued that load-bearing mineralized hard tissues, including bones, shells, and teeth, are nanocomposites, in which the mineral phase has nanoscale dimensions that ensure optimum strength and flaw tolerance. In particular, it has been claimed that the thickness of these brittle building blocks, being smaller than a critical size, h^*, of the order of tens of nanometers, renders them insensitive to the presence of crack-like flaws and enables them to achieve near-theoretical strength, which is why Nature employs nanoscale features in mineralized biological composites. We find this point of view, which Gao et al. and others have quoted in subsequent publications and presentations, unpersuasive and present several counterexamples which show that biological structures, as a result of being comprised of relatively fragile constituents that fracture at stress levels several orders of magnitude smaller than the theoretical strength, adopt various strategies to develop mechanical responses that enable them to mitigate catastrophic failure. Nanoscale structural features are not a result of an innate resistance to very high stresses.

Key words: Biological structures, crack bridging, flaw-intolerance, flaw-tolerance, nanoscale structures, toughening.

1. Cracks always weaken brittle solids

It has been realized since the seminal work of Griffith in (1921) that cracks or flaws always weaken brittle solids, and that increasing strength with decreasing specimen dimensions is not a question of flaw tolerance but of the decreasing probability that a "strength-defining" (Griffith) flaw is present in the area or volume being loaded. The argument of Gao et al. that nanoscale components in mineralized hard tissue could (and for toughness and strength of the overall structure are required to) attain (near) theoretical strength and flaw tolerance must therefore be rigorously examined. We will first present a classical elementary atomistic model that shows that a brittle structure containing a crack tens of nanometers long cannot achieve its theoretical strength, contrary to the argument of Gao et al.; this atomistic model is relevant to all brittle solids containing nanoscale defects, including mineralized hard tissues. We conclude that it is unlikely that if Nature's design were optimized, it would be

based on nanoscale features that can achieve – because of their size – near theoretical strength. We instead argue that load-bearing mineralized hard tissues, like many other natural composites, are associated with a diverse polyphase structure that is a consequence of the precipitation of minerals driven by chemical boundary conditions, rather than by an evolutionary plan. We will then buttress our argument using an example involving mollusk shells, which provide enhanced toughness and structural integrity by a hierarchical microstructure involving structure at five distinct length scales, and by bone, which utilizes continuous healing cycles to deal with fine scale fracture of otherwise fragile mineral constituents. The first example is drawn from a number of Ballarini and Heuer's previously published papers on the mechanical behavior of shells, while the second example involves new computational results that provide insight into the relevance of crack bridging mechanisms and R-curve testing of bone.

The argument of Gao et al. is based on an examination of the role of defects on the strength of homogeneous elastic nanoscale-thickness plates (which together with an organic "matrix" form a biological composite in many systems) by means of the Griffith fracture criterion (Griffith, 1921). Implicit in this analysis is the absence of plasticity (or other energy dissipative processes that could produce toughening) in the vicinity of the crack front (Should Gao et al. have incorporated plasticity near the crack front, then the cracked structure would in fact become less sensitive to the presence of the crack. However, the strength of such a structure would, at best, approach the bulk strength, f_t, which is orders of magnitude less than the theoretical strength). This situation corresponds to a vanishingly small characteristic size of the plastic zone, r_p, which, according to the Dugdale (1962) and the Barenblatt cohesive zone models, scales with the fracture toughness, K_{Ic}, and "bulk" strength, f_t (which is orders of magnitude smaller than the theoretical strength), as $r_p \sim (K_{Ic}/f_t)^2$.

Thus it is surprising that the analysis in question (Gao et al., 2003), on the basis of the Griffith criterion, predicts that a crack size exists for which a defective crystal is as strong as the perfect crystal. According to the Griffith criterion, the fracture strength of a crystal plate, σ_f, containing a surface crack of length a, can be related to its elastic modulus, E, fracture surface energy, 2γ, and thickness, h, by

$$\sigma_f \approx \alpha(a/h)\sqrt{\frac{E\gamma}{a}}, \tag{1}$$

where $\alpha(a/h)$ is a geometric constant of order unity (Equation (1) is the same as Equation (2) in Gao et al. However, in Equation (1) the crack length appears under the radical sign, so that α is defined differently than in ref. 1. This procedure implicitly assumes that the elastic solution employed to derive Equation (1), can be used at the theoretical stress, which corresponds to the point of instability in the interatomic force-separation law.). Gao et al. argue that the optimum size of a crystal is that at which the strength of the defective crystal equals the theoretical strength of the crystal, σ_{th}. This enables them to deduce a critical length scale, i.e. a length h^* below which the strength is unaffected by the presence of the crack

$$h^* \approx \alpha^2 \frac{\gamma E}{\sigma_{th}^2}. \tag{2}$$

While criteria of the form of Equation (2), which derive from the Dugdale and Barenblatt models, are quite frequently used in manufacturing as quality control criteria, the specificity of Gao et al.'s suggestion is the appearance of the theoretical strength, σ_{th}, in this equation. Assuming a set of parameters, namely $E = 100\,\text{GPa}$, $\sigma_{th} = E/30$, and $\gamma = 1\,\text{J/m}^2$, which at first glance appear reasonable, h^* is found to be $\sim 30\,\text{nm}$, which as described subsequently, corresponds to the thickness of but one of five (six) distinct structural features that comprise the shell of the Queen conch *Strombus gigas* (bone). Gao et al. proceed to validate their conclusion through a three dimensional finite element method based on the "virtual internal bond" model.

Some insight into these results can be gained from the approximate bond force models of the Lennard–Jones type (Jones, 1924)

$$\sigma(x) = \frac{E}{m-n}\left[\left(\frac{b_o}{x}\right)^n - \left(\frac{b_o}{x}\right)^m\right]. \tag{3}$$

Here $\sigma(x)$ represents the stress required to separate atoms by a distance x, b_o is the equilibrium (lattice) spacing of the atoms, and m and n are material constants. While the Lennard–Jones potential is not an accurate model for bond breaking of any particular material, it does provide a realistic scaling law relating defect size to strength. In particular, this model provides the following relationship between the fracture surface energy, the elastic modulus and the interatomic spacing

$$\frac{2\gamma}{Eb_o} = \frac{1}{(n-1)(m-1)}, \tag{4}$$

while the relationship between the theoretical strength and the elastic modulus is given by

$$\frac{\sigma_{th}}{E} = \frac{1}{m}\left(\frac{n}{m}\right)^{n/(m-n)}. \tag{5}$$

Combining this last equation with Equation (1) for the case of a Griffith (through thickness) crack, for which $\alpha = 1/\sqrt{\pi}$, we obtain

$$\frac{\sigma_f}{\sigma_{th}} = \frac{1}{\sqrt{\pi}}\frac{m}{(n/m)^{n/(m-n)}\sqrt{(n-1)(m-1)}}\sqrt{\frac{b_o}{a}}. \tag{6}$$

The theoretical strength normalized by the elastic modulus, the fracture strength divided by the theoretical strength, and the fracture surface energy divided by the product of the elastic modulus and lattice spacing, are listed in Table 1 for representative values of n and m for various types of chemical bonding. For σ_f to be equal to σ_{th}, Table 1 suggests that a would have to be $\sim 4b_o$, $\sim 8b_o$, and $\sim 3b_o$ for these types of bonding, and that cracks of the order of tens of nanometers, being two orders of magnitude larger than the lattice spacing b_o, must significantly reduce the fracture strength. This result is consistent with atomistic and quantum mechanics calculations performed on a variety of brittle materials (Belytschko et al., 2002; Mielke et al., 2004), where it was shown that removal of but a few atoms from the perfect structure significantly reduces strength. For the covalent material considered, we note that the fracture energy predicted by the Lennard-Jones model is four times lower than that assumed by Gao et al. It is unlikely that the strength of the mineral

Table 1. Parameter of Lennard-Jones model

Bond type	n	m	σ_{th}/E	$\sqrt{\frac{a}{b_o}}\frac{\sigma_f}{\sigma_{th}}$	$\frac{2\gamma}{Eb_o}$
Metallic	4	7	0.0677	1.96	0.0556
Ionic	2	10	0.0677	2.82	0.111
Covalent	8	12	0.0370	1.74	0.0130

phase in biological nanocomposites approaches the theoretical limit. For example, recent research into the multiscale mechanical properties of mineralized tissues show that *in situ* hydroxyapatite exhibits mechanical properties similar to a polycrystalline foam-like structure (Hellmich and Ulm, 2002; Hellmich et al., 2004), rather than an organized structure optimized for strength and flaw tolerance. As far as their crystal structure and morphology are concerned, mineralized hard tissues have much in common with many other natural inorganic composites; in particular a diverse polycrystalline structure that is a consequence of the precipitation of minerals driven by chemical boundary conditions, rather than by an evolutionary plan. Two examples of how biological structures deal with the inherent flaw sensitivity of the constituent materials are described next. The first example illustrates how the architectural designs of certain biological structures result in "graceful" failure due to effective and energy dissipating mechanisms. The second example suggests that other biological structures are not as successful at arresting the propagation of measurable cracks, and therefore rely on crack healing in order to survive mechanical forces without catastrophic failure.

2. High toughness via hierarchy

Various strategies are used by biological structures to achieve impressive mechanical strength and toughness, and these attributes are achieved despite low fracture strength of the nanoscale mineral constituents. Our first example involves the shell of the highly mineralized giant pink Queen conch, *Strombus gigas*. This structure contains 99% volume fraction of mineral and 1% volume fraction of organic "matrix", and achieves an extremely high level of toughening (as quantified through the work of fracture, the area under the load-displacement curve divided by the fracture surface area) and only moderate strength. What is important is that its high toughness is achieved using relatively weak and brittle aragonitic structural building blocks with dimensions of the order of tens of nanometers, via a hierarchical architecture that enables the development of energy-dissipating mechanisms operating at much larger length scales. These favorable mechanical properties are achieved with structural nanoscale features that fracture at stress levels that are two orders of magnitude lower than their theoretical strength.

A schematic of the shell's crossed-lamellar microarchitecture, which involves structure at five distinct length scales (Kessler et al., 1996; Kamat et al., 2000, 2004) is shown in Figure 1. The basic building blocks are high aspect ratio aragonitic internally twinned third order lamellae, whose elastic modulus is $\sim$100 GPa, which are about 60–100 nm by 100–380 nm in cross-section, many micrometers long and are

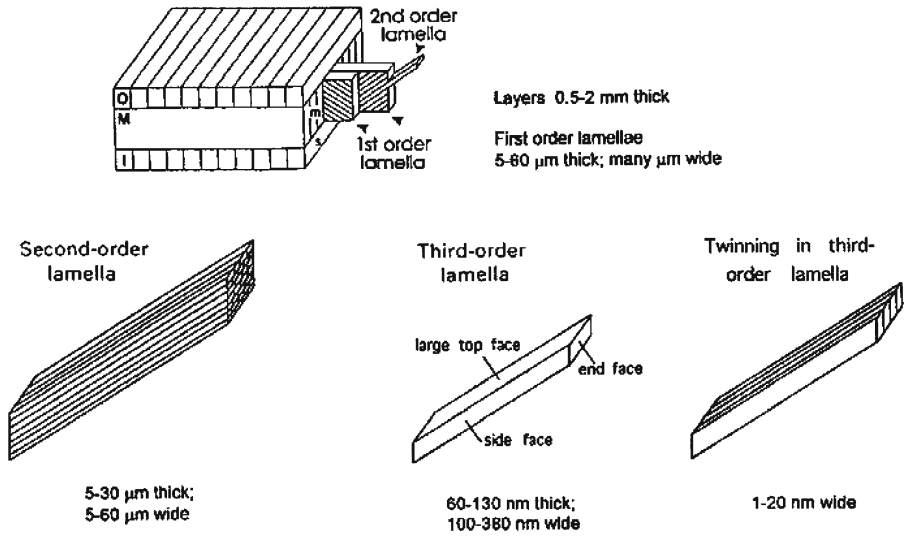

Figure 1. Microstructure of *Strombus giga*.

completely surrounded by an organic matrix. The third-order lamellae are assembled in a parallel arrangement into second-order lamellae (5–30 μm thick and 5–60 μm wide), which are also surrounded by organic matrix. The second-order lamellae are assembled in parallel to form the first-order lamellae (5–50 μm thick and many micrometers wide), which are assembled in an alternating $\pm 45^\circ$ parallel arrangement, separated by organic matrix, to form the coarsest macroscopic features, the inner, middle and outer layers. The coarsest features are arranged as 0°–90°–0° laminated plates, whose elastic modulus is ~ 40 GPa.

Ballarini and co workers have shown that the fracture resistance of this shell can be understood quantitatively by invoking two energy-dissipating mechanisms. Under bending loads, multiple "tunnel" cracks develop at the interfaces separating the first-order lamellae in the inner or outer layers, depending on which layer experiences the tensile stress. These cracks, which are arrested at the interface between these layers and the middle layer, are responsible for a twenty-fold increase in the work of fracture. This toughening is *completely independent* of the mechanical behavior of the nanoscale features of the shell! Instead, it relies on the existence of weak interfaces that are *millimeters long* and *tens of millimeters wide*. As the load is increased further, one or more of these cracks propagates along the weak organic interfaces in the middle layer. However, the crack propagation is resisted by bridging forces provided by the first-order lamellae perpendicular to the crack surfaces. This large scale bridging, operating at the millimeter scale, is the dominant energy dissipation mechanism, and is typical of ceramic matrix composites with weak interfaces. It is important to note that additional microscale cracking occurs in this structure; however, the details of this energy-dissipating mechanism have not been characterized explicitly, but have been incorporated in approximate crack-bridging models. Such a model was developed in Kessler et al. (1996) and Kamat et al. (2000, 2004), assuming that the crack front extends at the critical energy release rate of the organic matrix, J_m,

experimentally determined to be 0.7 MPa $\sqrt{m}$, while the crack opening displacements, u_y, are resisted by the traction, σ_b, resulting from the plate-like lamellae

$$\sigma_b = \beta u_y^{1/2}. \tag{7}$$

This crack resistance is operative up to a critical displacement, u_{cr}, or alternatively up to the tensile strength of the plates

$$\sigma_{cr} = \beta u_{cr}^{1/2}. \tag{8}$$

The energy release rate associated with the fiber bridging is (Rice, 1968) $J_b = \int_0^{u_{cr}} \sigma(u_y) du_y = \frac{2}{3}\beta u_{cr}^{3/2}$. Experiments were conducted to calibrate the parameters of the model, yielding $\beta_{shell} = 630\,\text{N/mm}^{5/2}$, $u_{cr}^{shell} = 0.005\,\text{mm}$, $J_b^{shell} = 0.15\,\text{N/mm}$, and $\sigma_{cr}^{shell} = 45\,\text{MPa}$. Significantly, the breaking stress predicted by this semi-empirical model, i.e. the nominal strength of the aragonitic plates, is orders of magnitude less than the theoretical strength, estimated by $\sigma_{th} = E/30$ to be ~3–4 GPa.

The relatively insignificant role played by the strength of the aragonite crystals in determining the toughness of the shell has been underscored recently by experiments (Kamat et al., 2000) which involved varying the toughness of the proteinaceous interfaces separating all structural features. At very low temperatures the fracture surfaces of the shell were relatively featureless, indicating very little of the fiber pull-out that is necessary for effective bridging, while at higher temperatures, the fiber pull-out and associated ductility increased significantly. In essence, the toughness relies not on the strength of the nanoscale features, but on the *toughness of the organic matrix*.

This example clearly shows that impressive structural toughness can be achieved in biological composites containing of flaw-intolerant nanoscale structural features (that fracture at stress levels several orders of magnitude smaller than the theoretical strength), through hierarchical structural designs that result in energy-dissipating mechanisms operating at much larger length scales. As discussed in the last section of this paper, the crack bridging parameters of the shell are associated with the favorable Aveston–Cooper–Kelly (ACK) limit (Aveston et al., 1971), where the crack-bridging ligaments remain intact as a crack propagates across the composite structure.

3. Survival via continuous healing cycles

The second example illustrates that bone, in part because its constituents have relatively large compliances, is associated (and must deal) with relatively ineffective crack bridging mechanisms. We demonstrate that bone is intolerant to the presence of cracks of macroscopic length, and thus mitigates the catastrophic structural failure that would result from the growth of cracks of measurable size through continuous biological resorption-regeneration healing cycles of the hydroxyapatite mineral phase. We argue that resorption reduces the stress intensity at sharp cracks and flaws, thereby reducing, by osteoclasis, the risk of crack propagation, and that this strategy of survival is little affected by the nanocomposite structure of the load-bearing mineral phase. As discussed subsequently, we believe that these new calculations have significant implications for the relevance of R-curve testing of bone structures.

We first estimate, assuming that no toughening mechanisms exist, the crack size that could be tolerated under a typical operating stress. The nominal fracture toughness of bone, which varies with the type and condition of bone, is of the order $K_c \sim 3\,\text{MPa-m}^{1/2}$, while the tensile strength σ_{max} is $\sim 250\,\text{MPa}$. (Currey, 2002) For an operating stress equal to a sizable fraction of the bending strength, say $\sigma = 100\,\text{MPa}$, the critical crack length is $a_{cr} = (K_c/\sigma)^2/\pi \approx 300\,\mu\text{m}$. This approximate calculation suggests that cracks with dimensions comparable to those of an osteon would lead, in the absence of crack-arresting mechanisms, to catastrophic failure by fracture. It is surmised that the osteons act as barriers to growth, and that bone eliminates, through remodeling, features containing small scale cracks that would otherwise grow to critical lengths. Recent compressive fatigue data of osteonal bone (O'Brien et al., 2005) confirm this conjecture, showing that microcracks greater than $100\,\mu\text{m}$ in length continue to grow despite the presence of osteons, and that microcracks greater than $300\,\mu\text{m}$ in length penetrate osteons and lead to failure. The calculations described next demonstrate that propagation of cracks of this length in bone, subjected to monotonically increasing loads, is resisted ineffectively only by crack-surface bridging forces arising from microstructural features.

Akkus and Rimnac (2001) conducted fracture mechanics experiments on irradiated and nonirradiated bone using compact tension specimens. In their study, they machined side grooves collinear with an initial notch such that the cracking that emanated from the notch-tip was forced to propagate transverse to the direction of the osteons. The load–displacement curve shown in Figure 2, which is representative of the curves they obtained for both irradiated and nonirradiated samples, was obtained under displacement control conditions. This data shows that bone is a strain-softening material, as is the shell of *Strombus gigas* (Kessler et al., 1996; Kamat et al., 2000; Hellmich et al., 2004). However, the constituents of bone are relatively compliant, and produce a relatively low elastic modulus; for Akkus and Rimnac's specimens, $E = 6.6$–$8.7\,\text{GPa}$. As discussed next, relatively low stiffness reinforcements are associated with relatively ineffective crack bridging of measurable cracks.

Fatigue and fracture of bone structures is a complex process, because the structure contains structural features spanning six distinct length scales; mineralized collagen molecules, fibrils, fibers, lamellae, osteons, and bone. In particular, the behavior of a very short crack, or cloud of cracks, contained within the smaller features, say the interfaces between fibrils, is different than cracks whose lengths span many osteons. The propagation of the former types of cracks would be dictated by the fracture resistance of the local environment at the crack tip, while propagation of long cracks would be determined by the fracture resistance of a different environment, as well as the bridging of the cracks by much larger ligaments. We do not address the initiation and growth of short cracks here. Rather we apply the bridging model discussed above to show that cracks of measurable length will propagate catastrophically in bone structures of any size.

Figure 2 also shows the experimental load–displacement curve predicted by the calibrated crack bridging model (isotropic elastic behavior and the cohesive model defined by Equation (7) were assumed to obtain order of magnitude estimates of physical parameters), which is based on nominal fracture toughness, $K_c = 3.1\,\text{MPa}\sqrt{m}$, critical energy release rate, $J_m = 1210\,\text{N/m}$, and fiber bridging

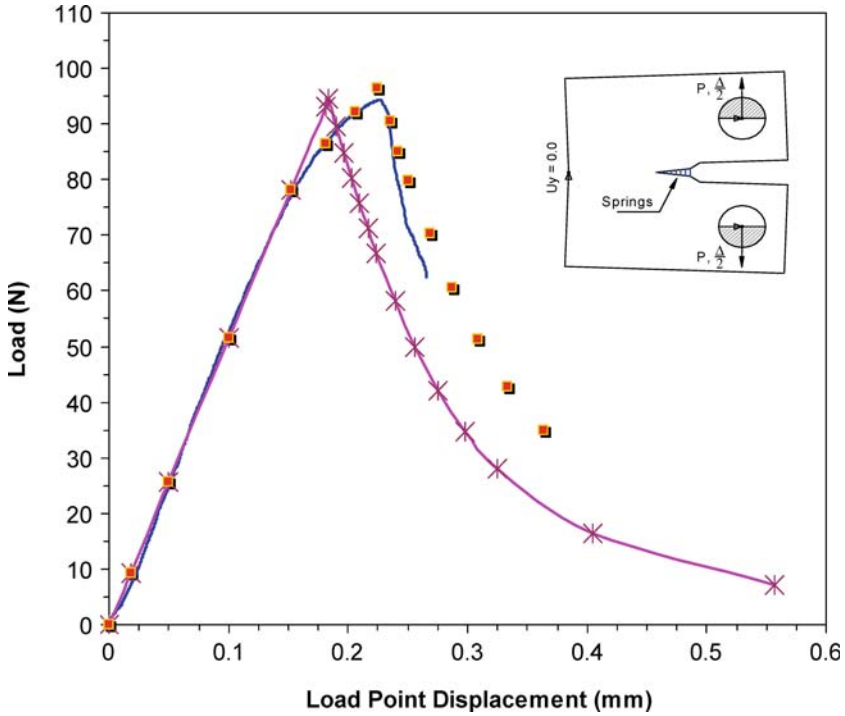

Figure 2. Load-displacement plot of a compact tension bone specimen. The solid curve corresponds to the experimental data. The discrete points correspond to the crack bridging model. The X-marked curve corresponds to Linear Elastic Fracture Mechanics.

energy, $J_b = 1020\,\text{N/m}$, $\beta = 224\,\text{N/mm}^{5/2}$, $u_{cr}^{bone} = 0.036\,\text{mm}$ and $\sigma_{cr}^{bone} = 43\,\text{MPa}$. It is remarkable that the micro and nanoscale features in bone fracture at stress levels similar to those in the shell of *Strombus gigas*, and that these are also much lower than the theoretical strength. Also shown on this plot is the load–displacement trace predicted using Linear Elastic Fracture Mechanics (LEFM), with the fracture toughness, $K_c = 3.8\,\text{MPa}\sqrt{m}$, calculated from the maximum load and the initial crack length. The level of toughening provided by crack surface bridging is relatively small.

Unlike the shell of *Strombus gigas*, the crack bridging parameters of bone are associated with small-scale bridging phenomena, and are far from those required to approach the ACK limit. This suggests that bone is intolerant to the presence of cracks of macroscopic length, regardless of a possibly optimal nanocomposite structure, in marked contrast to the model suggested by Gao et al. (2003) To substantiate our argument, we used the calibrated model to estimate the nominal tensile strength of a beam specimen of bone, with length L, depth $h = L/10$, and unit thickness, containing an initial notch of length $a_o = 0.075\,\text{h}$. The tensile strength as a function of beam size (the maximum stress achieved) is shown in Figure 3 together with the strength of the same beam in the absence of crack bridging forces (the LEFM model with a fracture toughness equal to $K_c = 3.1\,\text{MPa}\sqrt{m}$). Far from being optimized, crack bridging mechanisms in bone increase the nominal strength only marginally. Hence, bone, in contrast to other mineralized composites, appears not to be able to prevent unstable crack propagation of cracks of macroscopic length by means

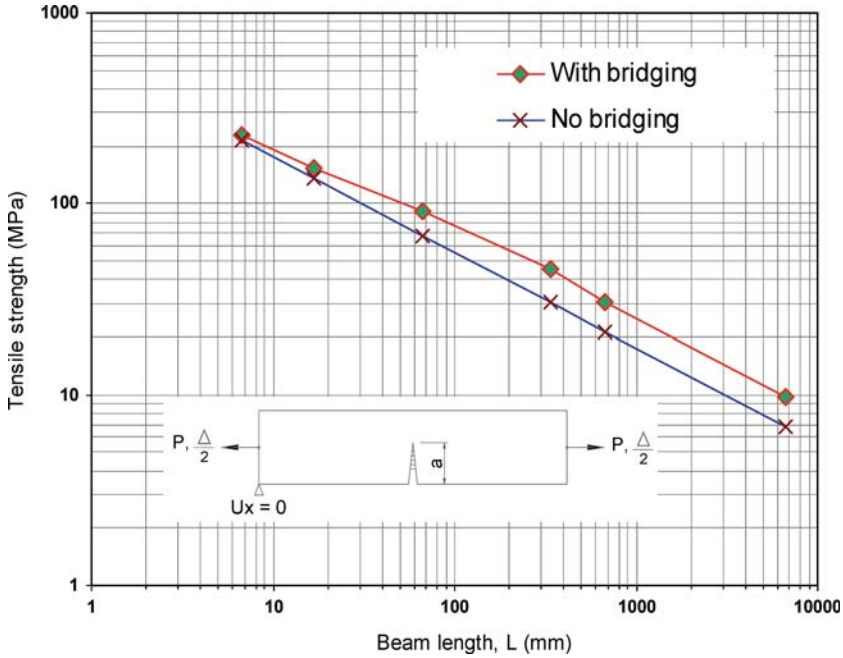

Figure 3. Tensile strength of bone as functions of specimen size predicted by the crack bridging model and LEFM.

of optimized microstructural features, and would necessarily fail even under normal physiological conditions if such cracks were present.

These results suggest that experimental R-curves for bone need to be interpreted with caution. While the propagation of a crack from a relatively long traction-free precrack will undoubtedly be associated with a rising R-curve, the results presented above suggest that in a bone structure, the precrack could not possibly develop; cracks longer than a few hundred microns will grow catastrophically, and the R-curve information may not be of practical significance.

The absence of cracks of such size in bones hints towards the intimate coupling between cell-mediated resorption processes and damage accumulation and fracture induced by loading that effectively prevents such cracks from developing. Indeed, it is well known that zones with diffuse damage and/or microcracks undergo increased resorption (Burr et al., 1985; Schaffler and Jepsen, 2000), although the mechanisms are still a matter of debate. The characteristic size of osteoclasts, the cells specialized in resorbing mineralized bone, is on the order of 50 μm. This is of a similar order as the cracks, which – by resorption – are prevented from propagating. Resorption reduces the stress intensity at sharp cracks and flaws, thereby reducing, by osteoclasis, the risk of crack propagation. The newly generated surface is opened to osteoblast cells, and concurrent osteogenesis (Silva and Ulm, 2002).

In conclusion, prevention of failure in bone appears to emanate from a strategy of survival that is achieved by a finely tuned coupling between biochemistry, mechanotransduction, damage and fracture. This strategy is independent of the nanocomposite structure of the load-bearing mineral phase and appears to operate for crack lengths substantially larger than the nanoscale.

4. Length scales

We have demonstrated through two examples that the material length scale introduced by Gao et al., $h^* \approx \alpha^2(\gamma E/\sigma_{\text{th}}^2)$, is not (generally) relevant to the toughening of hierarchical biological structures. Instead, the crack bridging phenomena that is active in these structures are associated with much larger length scales and involve scaling laws that can be explored using the parameters J_{m}, J_{b}, β and the elastic modulus E (Cox and Marshall, 1994; Hellmich et al., 2004); these determine the toughness and notch sensitivity, and whether failure occurs as a result of catastrophic or non-catastrophic crack propagation. Specifically, the material length scales are a_{m} and a_{s} (Cox and Marshall, 1994). The first corresponds to the amount of growth necessary to approach the ACK limit (Aveston and Cooper, 1971), while the second corresponds to the length of the bridging zone in a very long crack. Both parameters provide insight into the type of (bridged) crack propagation that occurs in composite plates of width h, whether they are unnotched or contain a notch of length, c. First, non-catastrophic failure gives way to catastrophic failure if J_{m} exceeds J_{b}. Second, the effectiveness of the fibers increases with increasing h/a_{m}. If the width of a specimen is much less than a_{m}, then bridging effects are negligible, even though the bridging ligaments may be intact all along the crack wake. Third, if $c \gtrsim a_{\text{m}}$, then crack growth from a notch is stable. On the other hand, if the specimen contains a notch that is much shorter than a_{m}, crack growth is unstable immediately (or shortly after) the crack emerges from the notch. Finally, if $a_{\text{m}} << a_{\text{s}}$, then the ACK limit will be reached in a sufficiently large specimen.

For the shell of *Strombus gigas*, $a_{\text{s}} \sim 25\,\text{mm}$, $a_{\text{m}} \sim 1.3\,\text{mm}$, $h \sim 10\,\text{mm}$, and the multiple tunnel cracks that are arrested at the interface between the weak and tough layers act as initial notches of length $c \sim 5\,\text{mm}$. These parameters indicate that the conch shell is associated with all of the favorable characteristics described above.

A cracked or notched piece of bone, on the other hand, is far from achieving graceful failure, because J_{m} (1210 N/m) exceeds J_{b} (1020 N/m), and a_{m} (850 mm) is comparable to a_{s} (540 mm).

5. Conclusions

The examples presented in this paper illustrate that biological structures use various strategies to avoid mechanical failure, and that these strategies do not rely on flaw tolerance of nanoscale structural features. On the contrary, biological structures can achieve impressive toughness and strength using nanoscale features with relatively low strength.

References

Gao, H., Ji, B., Jager, I.L., Arzt, E. and Fratzl, P. (2003). PNAS **100**, 5597–5600.
Griffith, A.A. (1921). *Phil. Trans. Roy. Soc. A* **221**, 163–197.
Dugdale, D.S. (1962). *Journal of the Mechanics and Physics of Solids* **8**, 100–104.
Barenblatt, G.I. (1962). In: *Advances in Applied Mechanics,* Vol. VII, pp. 55–129.
Jones, J.E. (1924). *Proc. Roy. Soc. of London* **106A**, 441–462; (1924). *Proc. Roy. Soc. of London* **106A**, 463–477.

Mielke, S.L., Troya, D., Zhang, S., Li, J.L., Xiao, S., Car, R., Ruoff, R.S., Schatz, G.C. and Belytschko, T. (2004). *Chemical Physics Letters* **390**(4–6), 413–420.

Belytschko, T., Xiao, S.P., Schatz, G.C. and Ruoff, R.S. (2002). *Phys. Rev. B* **65**, Article 235430.

Hellmich, C., Ulm, F.-J. (2002). *Journal of Biomechanics*, **35**(9), 1199–1212.

Hellmich, C., Barthelemy, J.-F., Dormieux, L. (2004). *European Journal of Mechanics* A-Solids **23**, 783–810.

Kessler, H., Ballarini, R., Mullen, R.L., Kuhn, L.T. and Heuer, A.H. (1996). *Computational Materials Science* **5**, 157–166.

Kamat, S., Su, X., Ballarini, R. and Heuer, A.H. (2000). *Nature* **405**, 1036–1040.

Kamat, S., Kessler, H., Ballarini, R., Nassirou, M. and Heuer, A.H. (2004). *Acta Materialia* **52**, 2395–2406.

Rice, J.R. (1968). *Journal of Applied Mechanics* **35**, 379–386.

Aveston, J., Cooper, G.A. and Kelly, A. (1971). *Conf. Proc. 15*, National Physical Laboratory, IPC Science and Technology Press.

Currey, J.D. (2002). *Bones: Structure and Mechanics*, Princeton University Press, Princeton.

O'Brien, F.J., Taylor, D. and Lee, T.C. (2005). *J. Orthopaedic Research* **23**, 475–480.

Akkus, O. and Rimnac, C.M. (2001). *Journal of Orthopaedic Research* **19**, 927–934.

Schaffler, M.B. and Jepsen, K.J. (2000). *International Journal of Fatigue* **22**(10), 839–846.

Burr, D.B., Martin, R.B., Schaffler, M.B. and Radin, E.L. (1985). *Journal of Biomechanics* **18**(3), 189.

Silva, E.C. and Ulm, F.-J. (2002). In: (edited by Karihaloo, B. L) *Proceedings of IUTAM Symposium on Analytical and Computational Fracture Mechanics of Non-Homogeneous Materials*, Kluwer Acad. Pub., London, pp. 355–366.

Cox, B.N. and Marshall, D.B. (1994). *Acta Metall. Mater.* **42**, 341.